Moderate-Resolution Imaging Spectroradiometer ocean color polarization correction

Gerhard Meister, Ewa J. Kwiatkowska, Bryan A. Franz, Frederick S. Patt, Gene C. Feldman, and Charles R. McClain

The polarization correction for the Moderate-Resolution Imaging Spectroradiometer (MODIS) instruments on the Terra and Aqua satellites is described. The focus is on the prelaunch polarization characterization and on the derivation of polarization correction coefficients for the processing of ocean color data. The effect of the polarization correction is demonstrated. The radiances at the top of the atmosphere need to be corrected by as much as 3.2% in the 412 nm band. The effect on the water-leaving radiances can exceed 50%. The polarization correction produces good agreement of the MODIS Aqua water-leaving radiance time series with data from another, independent satellite-based ocean color sensor, the Sea-Viewing Wide Field-of-View Sensor (SeaWiFS). © 2005 Optical Society of America

OCIS codes: 260.5430, 120.5800, 280.0280, 010.0010.

1. Introduction

NASA's Earth Observing System (EOS) satellites Terra[1] and Aqua[2] each carry a Moderate-Resolution Imaging Spectroradiometer[3] (MODIS) that produces global coverage every 2 days with a nadir spatial resolution of 1 km for the nine ocean color bands. The Ocean Biology Processing Group[4] (OBPG) at NASA's Goddard Space Flight Center has been responsible for processing the MODIS ocean color data since early 2004. The authors of this paper are members of that group. Our goals in this paper are to describe the implementation of the results of the prelaunch polarization characterization and to demonstrate the importance of the polarization correction to the MODIS ocean color products.

The wavelengths of the MODIS ocean color bands are given in Table 1. MODIS scans the Earth from its polar orbit, with a scan perpendicular to the flight direction. The MODIS polarization sensitivity was characterized prelaunch for several viewing angles for the ocean color bands. Interactions between polarization and the response versus viewing angle are discussed by Knight *et al.*[5]

Normalized water-leaving radiances (L_{WN}; see Wang *et al.*[6] for a definition) are the basic ocean color products. The atmospheric correction is the main challenge when one is converting measured top-of-atmosphere (TOA) radiances (I_m) to L_{WN}. The polarization components of the TOA radiances are modeled separately for Rayleigh scattering from the atmosphere and glint from the ocean surface; then they are summed to provide total polarization components (Q_t and U_t; see below). Rayleigh and glint radiances are modeled by the successive-order-of-scattering method applied to the vector radiative transfer equation to account for polarization, assuming a Rayleigh-scattering atmosphere overlying a Fresnel-reflecting ocean surface.[7] The ocean surface's roughness is derived from the wind speed.[8] The measured TOA radiances are corrected by use of the instrument's prelaunch polarization characterization and the modeled polarization components of the TOA radiances (see Fig. 1), which assumes that polarization components caused by aerosol scattering and water-leaving radiances are negligible. We expect that future algorithms will allow us to improve on this assumption.

The degree of polarization of the modeled TOA radiance varies strongly with scattering angle, typically from 0% to 70%. The response of the MODIS Aqua varies by as much as ±5.4% for completely polarized light (depending on the direction of the electric field vector relative to the MODIS); see Table 2. The av-

G. Meister (meister@simbios.gsfc.nasa.gov) is with Futuretech Corporation, Greenbelt, Maryland 20770. E. J. Kwiatkowska, B. A. Franz, and F. S. Patt are with Science Applications International, Beltsville, Maryland 20707. G. C. Feldman and C. R. McClain are with the National Aeronautics and Space Administration, Goddard Space Flight Center, Greenbelt, Maryland 20771.

Received 8 December 2004; revised manuscript received 8 April 2005; accepted 13 April 2005.

0003-6935/05/265524-12$15.00/0

© 2005 Optical Society of America

Table 1. Center Wavelengths and Bandwidths for the MODIS Aqua Ocean Color Bands and the SeaWiFS[a]

MODIS Band Number	MODIS Center Wavelength (nm)	MODIS Bandwidth (nm)	SeaWiFS Center Wavelength (nm)	SeaWiFS Bandwidth (nm)
8	412	15	412	20
9	443	10	443	20
10	488	10	490	20
11	531	10	510	20
12	551	10	555	20
13L[b]	667	10	670	20
14L	678	10		
15	748	10	765	40
16	870	15	865	40

[a]Sea-Viewing Wide Field-of-View Sensor.
[b]L denotes low-gain output.

Table 2. Measured MODIS Aqua Polarization Amplitude p_a [Eq. (13)], Estimated Standard Uncertainty ($k = 1$) of the Modeled Polarization Sensitivity σ_P [Eq. (11)], and MODIS Aqua Polarization Phase Angle δ [Eq. (1)][a]

Band	Mean(p_a)	Max(p_a)	σ_P	Mean(δ) (°)
8	0.045	0.054	0.002	−10
9	0.023	0.031	0.005	−15
10	0.011	0.011	0.01	−8
11	0.009	0.013	0.008	−23
12	0.013	0.020	0.006	83
13L	0.008	0.008	0.01	−34
14L	0.009	0.012	0.01	−9
15	0.005	0.007	0.01	18
16	0.018	0.025	0.005	84

[a]The statistics for p_a and δ are calculated for the prelaunch measurement viewing angles.

erage contribution of Rayleigh scattering to TOA radiances with ≥70% degree of polarization is ~80% at 412 nm. Thus, for the MODIS, the measured TOA radiance must be corrected by as much as ±3.0% (=±5.4% × 0.7 × 0.8). The desired total accuracy for the TOA radiances of the ocean color bands is 0.5% or better; thus the need for an accurate polarization correction is obvious. The vicarious calibration used for ocean color sensors[10] can correct constant calibration offsets only, not variable effects such as polarization. Comparisons with data from other satellite sensors are a useful validation tool, but, especially for the atmospheric correction bands (15 and 16), these comparisons are problematic. Thus an accurate prelaunch polarization characterization is essential in meeting the ocean color data quality requirements.

The prediction of the TOA polarization components has been described by Gordon *et al.*,[9] as has the basic correction algorithm. We follow the conventions and notation used there. In this paper we present a slightly improved algorithm. The focus of this paper is on the analysis of the prelaunch characterization and its effect on the MODIS Aqua ocean color data products. Because of an incorrect interpretation of the prelaunch characterization, an erroneous polarization correction was applied for the ocean color products distributed before February 2004. This error severely compromised a significant portion of the MODIS ocean color products. We show the improvement gained by application of the rectified polarization correction by comparing the water-leaving radiances from the MODIS Aqua with those from the SeaWiFS,[11] which has a nominal polarization sensitivity of ~0.25%, a factor of 20 less than the maximum polarization sensitivity of the MODIS.

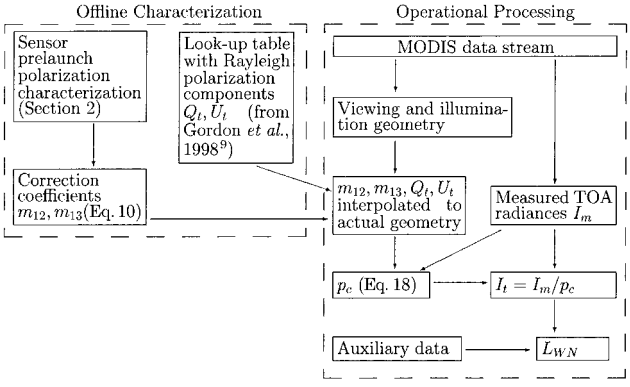

Fig. 1. Flow chart of the MODIS Aqua ocean color polarization correction.

2. Prelaunch Polarization Characterization

The MODIS polarization sensitivity was characterized prelaunch by Raytheon Santa Barbara Remote Sensing (SBRS), Goleta, Calif. The setup is shown in Fig. 2. The polarization spectral assembly (PSA) produces linearly polarized light, with the direction of the electric field vector E given by polarizer angle β. The PSA contains an Ahrens prism and a collimating mirror. The primary light path is from the PSA (from the light source through the Ahrens prism, to the collimating mirror) into the MODIS (reflected or transmitted by MODIS internal mirrors and beam splitters, passing the focal plane filters, to the detectors). The PSA must provide a homogeneous, completely polarized light field for the large MODIS scan mirror. The reflecting surface of the MODIS scan mirror is an ellipse with a width of 21 cm and a maximum length of 58 cm,[12] depending on the angle of incidence (AOI).

The PSA was rotated with an angular range from $\beta = -180°$ to $\beta = +180°$ (the plane of polarization or direction of vibration of the electric field vector is the same for $\beta = -180°, 0°, +180°$). These measurements were repeated for several viewing angles of the MODIS relative to the PSA ($-45°, -22.5°, 0°, +22.5°, +45°$). SBRS delivered preformatted data to the MODIS characterization support team, which provides the data to the MODIS science teams.

The AOI on the scan mirror varies from 10.5° to 65°, corresponding to viewing angles on the spacecraft of −55° and +55°, respectively.[13] A MODIS scan is divided into 1354 frames, with frame 1 corresponding to an along-scan viewing angle of −55° and frame

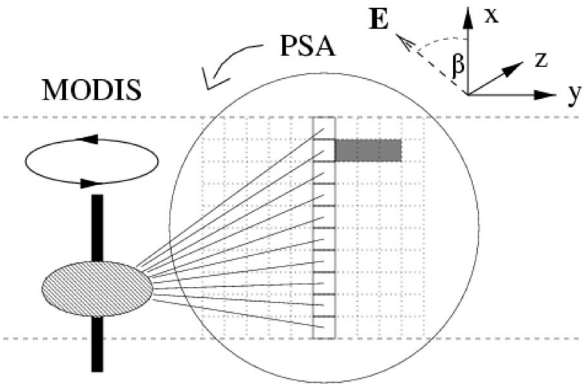

Fig. 2. MODIS viewing the PSA. The only MODIS components shown are the scan mirror (hatched ellipse) and its rotation axis (solid vertical bar). The scan mirror rotates in the direction indicated by the arrows above the rotation axis. The MODIS scans frames from the right side of the figure to the left. The horizontal dashed lines show the edge of the scan line, which contains ten detectors for the ocean color bands. The angular separation between the detectors (indicated by the ten solid lines running from the MODIS to the PSA) is largely exaggerated in this figure. The x, y, and z axes are the right-handed sensor coordinate system as defined by SBRS; the x axis points into the MODIS flight direction, and the z axis, toward nadir. The circle is the PSA aperture. The PSA can be rotated about the z axis. The bent arrow next to the PSA shows the direction of increasing polarizer angles β. For β = 0°, electric field vector $\boldsymbol{E}$ is parallel to the x axis. The MODIS viewing angle is given by the angle between the z axis and the ten solid lines. The MODIS was rotated about its x axis to measure at different viewing angles. An example for the calculation of the measured radiance is shown for detector 9: If the average of the three filled squares is the highest average of three consecutive frames for detector 9, this average will be taken as the measured radiance for the current β, viewing angle, detector, band, and mirror side. The combination of ten along-track detectors and the rotation of the scan mirror creates an image of the PSA aperture, which is shown in Fig. 3 for three rotation angles β.

1354 to +55°. Ten detectors measure radiances simultaneously for each ocean color band for every frame of the MODIS. Small angular differences (≈0.08°) in the along-track direction of the field of view between the detectors result in a 10 × 1354 image for every scan line; see Fig. 2. Thus the polarization sensitivity of the MODIS is a function of viewing angle, detector number, mirror side, and band.

Let I_t be the radiance that would be measured by a sensor with no polarization sensitivity. For a sensor with polarization sensitivity, let δ be the rotation angle β of the PSA at which the measured signal is highest. Then the measured signal will be lowest for rotation angles β = δ ± 90° and highest again for β = δ ± 180°. Thus the expected result of the polarization measurements is a signal with two cycles over the range of rotation angles β of the polarizer from −180° to +180°. According to Waluschka,[14] the expected measured radiance $I_m(\beta)$ can be described by

$$I_m(\beta) = I_t[1 + p_a \cos(2\beta - 2\delta)], \tag{1}$$

where p_a is the polarization amplitude. Integrating Eq. (1) over β,

$$\int_{-180°}^{180°} I_m(\beta)\mathrm{d}\beta = \int_{-180°}^{180°} I_t[1 + p_a \cos(2\beta - 2\delta)]\mathrm{d}\beta = I_t \int_{-180°}^{180°} \mathrm{d}\beta + 0, \tag{2}$$

shows that I_t can be approximated by the mean of the measured radiances by

$$I_t \approx \frac{1}{n} \sum_{i=1}^{n} I_m(\beta_i) \tag{3}$$

because the sampling interval for β covers the polarization cycle homogeneously (β was varied in 15° intervals for the MODIS Aqua prelaunch measurements and in 30° intervals for the MODIS Terra). In relation (3), n is the number of rotation angles β_i at which measurements were made. Note that $I_m(\beta = -180°)$ and $I_m(\beta = 180°)$ should be used only as one averaged value to avoid overweighting the values at β = ±180°.

Homogeneous illumination of an area the size of the MODIS scan mirror with linearly polarized light for all rotation angles of the polarizer (β) is a huge challenge. Figure 3 shows the MODIS Aqua band 8 measurements for three β angles as a function of detector and frame number. Rotating the polarizer by Δβ = 180° should not change the measured signal. Figure 3 shows that the measurements for β = −180° and β = 0° differ significantly; this indicates a problem with the quality of the prelaunch measurements. The case shown is the worst case; the other MODIS bands are more consistent. We believe that possibly the output of the PSA is spatially inhomogeneous at shorter wavelengths. SBRS staff members, however, do not believe that the PSA could have produced such a pattern. The reason for this anomaly remains unresolved.

The measured radiance for each polarizer angle $I_m(\beta)$ is calculated as the average radiance of the three highest consecutive frames (Fig. 2) for each detector, following a recommendation by the MODIS characterization support team. Other options for calculating the measured radiance were explored but did not lead to a significant improvement of the final results. The polarization amplitudes retrieved with the method described above agree well with those reported by SBRS.[15]

In this paper the radiances measured during the prelaunch polarization characterization are normalized to the mean radiance over all angles β and are referred to as I_m^N (dimensionless):

$$I_m^N(\beta) = I_m(\beta)/I_t, \tag{4}$$

where I_t is calculated with relation (3).

Figure 4 shows I_m^N for all detectors of bands 8 and 16 for those three polarizer angles (β = −180°, 0°, 180°), which should yield identical I_m^N. It can be

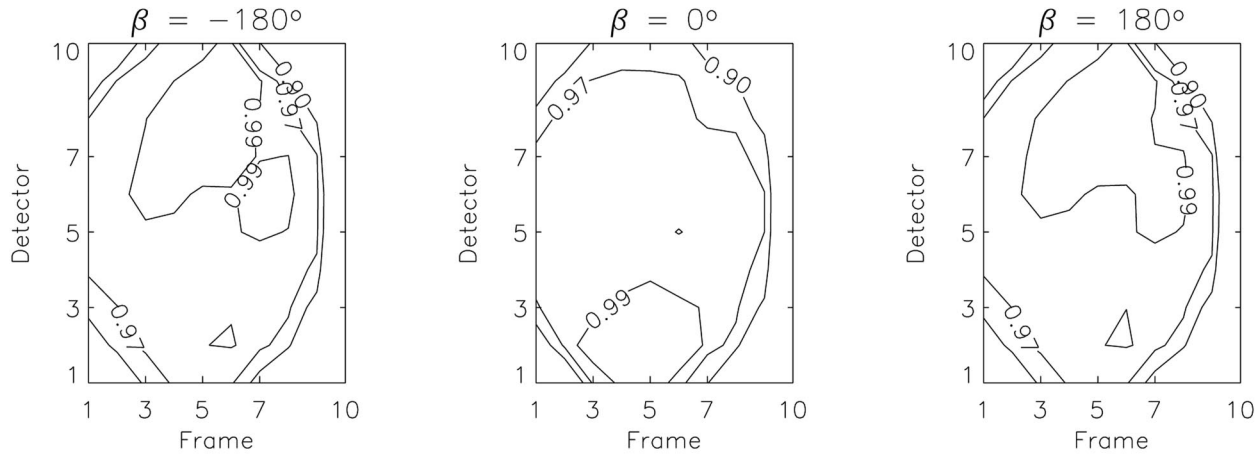

Fig. 3. Left, contour plot of the MODIS Aqua band 8 measurements of the PSA aperture for a viewing angle of 45°. Each measurement originates from one of the 100 squares shown in Fig. 2. The measured values have been normalized to the maximum in each of these three figures. Frame numbers 1–10 on the x axis refer to a subset of the complete MODIS scan (1354 frames). The detector numbers on the y axis are in product order. The x axis is parallel to the x axis in Fig. 2; the y axis is antiparallel to the y axis in Fig. 2.

seen that, for band 16, the three measurements for each detector agree within 1%. However, the measurements for band 8 agree within 1% only for detector 1. For detector 10 they differ by ~5%. This indicates that the quality of the prelaunch measurements differs among the detectors. It is worth noting that differences in the polarization sensitivities among the detectors are expected to be caused mainly by angular differences within the MODIS optics that are due to the small angular differences of the along-track viewing angles (Fig. 2) and not by characteristics of the detectors themselves. Therefore it was decided to choose, for each band, viewing angle, and mirror side, the detector whose measurements seem to be least influenced by measurement artifacts. The polarization correction coefficients derived from this detector were then applied to all ten detectors. The selection criteria and the resultant choices have been documented by Meister.[16] The most important criterion is how close the measurements are to the expected two-cycle variation described by Eq. (1). Recent results from a ray tracing simulation[17] for band 8 indicate that the variation of polarization sensitivity among detectors is much smaller than the variation observed in the prelaunch measurements, which confirms our approach of ignoring differences in the measured polarization sensitivities among detectors.

Measured radiances I_m^N for the chosen detectors as a function of β are shown in Fig. 5 for bands 8, 11, 15, and 16. The four figures shown are representative of the main quality issues of the MODIS Aqua prelaunch polarization characterization measurements:

- Even after only the best detector has been selected, the measured radiances for negative β are on average lower than for positive β for all bands. It is

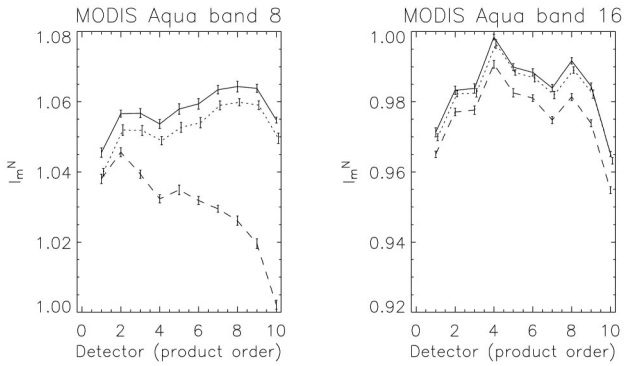

Fig. 4. Measured radiances I_m^N of the MODIS Aqua as a function of detector number, for a viewing angle of 45°, bands 8 and 16, mirror side 1. The solid, dashed, and dotted curves are for β = −180°, 0°, 180°, respectively. The error bars are the standard deviations over ten scans, averaged over the three frames with the highest signal for each detector.

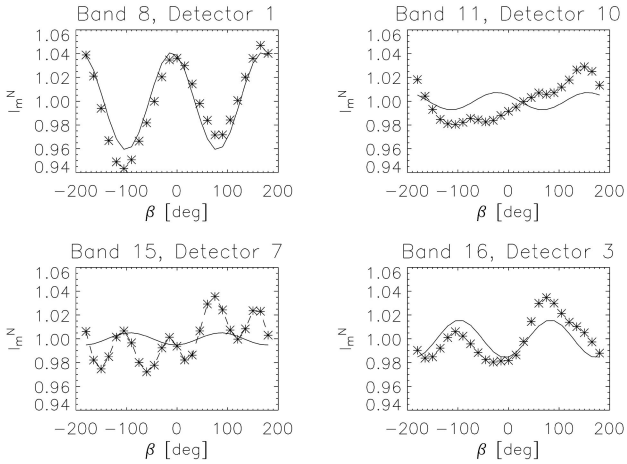

Fig. 5. Prelaunch polarization characterization measurements for MODIS Aqua bands 8, 11, 15, and 16. The stars show the measured radiances I_m^N for a viewing angle of 0° as a function of β angle. Solid curves show the retrieved two-cycle component [cf. Eq. (11)]. The dashed curve connects the band 15 measurements to accentuate the four-cycle pattern.

possible that these errors cancel when the polarization coefficients are derived, so the net effect might be minor.

- For some bands there is no clear two-cycle pattern, e.g., band 11 in Fig. 5. This indicates that the measurement uncertainty is similar in magnitude to the polarization sensitivity of the MODIS in some bands.
- Some near-infrared bands (13–15) have a four-cycle pattern rather than a two-cycle pattern.

The four-cycle pattern has been analyzed extensively for the MODIS Terra.[14,18] It has been shown that this phenomenon is caused by a secondary light path, where light that has been polarized by the PSA is reflected from the MODIS focal plane filters back to the PSA and then back into the MODIS again. Young *et al.*[18] showed that the four-cycle pattern in the MODIS Terra prelaunch measurements can be removed by use of Fourier analysis to extract the two-cycle component. Figure 6 shows the retrieved intensities of the two-cycle Fourier component and the four-cycle Fourier component for band 15 for all ten detectors. It can be seen that, for Terra, the two-cycle component is lowest for detectors for which the four-cycle component is highest and vice versa. This could be an indication that the four-cycle pattern is interfering with the correct retrieval of the two-cycle component. Some bands with no four-cycle pattern, however, have a detector-dependent two-cycle pattern similar to that of band 15.

For the MODIS Aqua, the detector-dependent pattern of the two-cycle component is opposite that of the MODIS Terra: for the MODIS Terra, detectors 1 and 10 have higher two-cycle components than detectors 5 and 6, whereas for the MODIS Aqua the two-cycle components of detectors 1 and 10 are lower than (or comparable to) those of detectors 5 and 6; see Fig. 6. Furthermore, the four-cycle pattern is much stronger in the MODIS Aqua than in the MODIS Terra. It is even stronger than the two-cycle component, which seems to conflict with the argument that a secondary light path causes the four-cycle pattern. Specifically, how can the intensity from the primary light path (two-cycle pattern) be weaker than the intensity from the secondary light path (four-cycle pattern)? Nevertheless, lacking a better understanding of all the processes involved, we use the method suggested by Young *et al.*[18] here as well. It should be noted that the authors do not want to imply that the secondary light path theory is wrong, but we believe that it does not describe all the characteristics of the four-cycle pattern in the MODIS Aqua, and the retrieval of the two-cycle component from the prelaunch measurements with Fourier analysis may be problematic.

Although MODIS Terra prelaunch measurements were made at a coarser resolution of β, the quality is possibly superior to that of the MODIS Aqua measurements with respect to the clarity of the two-cycle signal. The MODIS Terra and MODIS Aqua share the same design and the same prescriptions for the optical surfaces. Therefore the differences in their optical characteristics should be due only to variations in the fabrication process, which were expected to be small.

A comparison of the polarization amplitudes p_a for bands 8 and 16 for Aqua and Terra is presented in Fig. 7. It can be seen that p_a for these two bands increases with viewing angle (the viewing angle is proportional to the AOI on the scan mirror). There is a significant difference of almost 0.01 between the two mirror sides for Terra at large viewing angles for bands 8 and 16. Because any measurement artifacts should affect the two mirror sides similarly, this difference is probably real. There is also a difference of ~0.01 between the Aqua and Terra polarization amplitudes in band 16. For bands 9–15, the difference between Aqua and Terra varies from 0 to 0.015, with the Terra polarization amplitude usually being higher.

3. Polarization-Correction Algorithm

The Stokes vector components of the polarized radiance at the TOA for linearly polarized light (Q_t for horizontal–vertical polarization; U_t for ±45° polarization) are calculated in the MODIS processing code

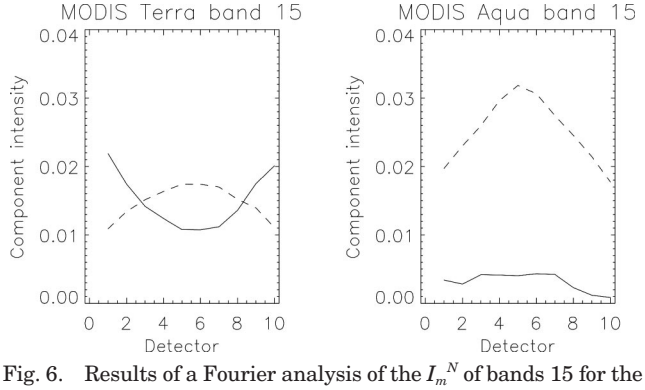

Fig. 6. Results of a Fourier analysis of the I_m^N of bands 15 for the MODIS Terra and MODIS Aqua for a viewing angle of 45°. The solid curves show the intensities of the retrieved two-cycle component [p_a in Eq. (13)]; the dashed curves show the intensities of the retrieved four-cycle component.

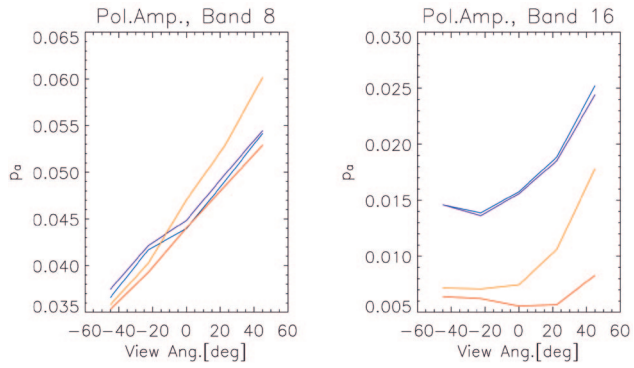

Fig. 7. Polarization amplitudes p_a derived from Eq. (13) for bands 8 and 16 for the MODIS Aqua (blue curve, mirror side 1; purple curve, mirror side 2) and MODIS Terra (orange curve, mirror side 1; red curve, mirror side 2).

in a reference system relative to the ocean surface normal. The polarization correction parameters are calculated for Stokes vectors relative to a reference plane fixed with respect to the instrument. The transformation between these two reference planes is given by Gordon *et al.*[9] by the angle α. For the prelaunch laboratory measurements, α can be set to zero. On orbit, α is 180° for the first half of the MODIS Aqua scan and 0° for the second half of the MODIS Aqua scan and varies for view angles close to nadir. The basic formula for the polarization correction is Eq. (7) from Ref. 9:

$$I_m = I_t\{1 + m_{12}[\cos(2\alpha)Q_t/I_t + \sin(2\alpha)U_t/I_t] + m_{13}[-\sin(2\alpha)Q_t/I_t + \cos(2\alpha)U_t/I_t]\}, \quad (5)$$

which simplifies to the following equation with $\alpha = 0°$ for the laboratory measurements:

$$I_m = I_t[1 + m_{12}Q_t/I_t + m_{13}U_t/I_t]. \quad (6)$$

For completely linearly polarized light, Q_t and U_t are given by[19]

$$Q_t = I_t \cos 2\gamma, \quad (7)$$

$$U_t = I_t \sin 2\gamma, \quad (8)$$

where γ is defined in Fig. 8. Rotation angle β of the polarizer used by SBRS to describe the prelaunch measurements is related to angle γ used in the polarization correction algorithm of Gordon *et al.*[9] by

$$\gamma = -\beta + 90°. \quad (9)$$

Equation (9) is incorrect in versions of the MODIS processing code before 2004 (referred to by the Goddard Distributed Active Archive Center[20] as versions 4 and earlier for the MODIS Terra and as versions 3 and earlier for the MODIS Aqua), effectively leading to polarization correction coefficients m_{12} and m_{13} with wrong signs. The rectified data set for the MODIS Aqua has been available since May 2004 from the OBPG Web site.[4]

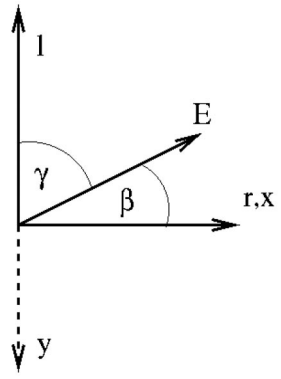

Fig. 8. Electric field vector E in the MODIS ocean color processing code coordinate system (r, l) and the MODIS sensor coordinate system (x, y, z) as defined by SBRS. The propagation direction of light is from the figure toward the viewer, opposite the z axis of the sensor coordinate system (not shown in this figure, but in Fig. 2).

For the laboratory measurements Eq. (6) can be transformed to

$$I_m(\gamma)/I_t = (1 + m_{12}\cos 2\gamma + m_{13}\sin 2\gamma). \quad (10)$$

We derived the quantities m_{12} and m_{13} by fitting the right-hand side of Eq. (10) to the measured radiances I_m^N. The resultant modeled polarization sensitivity P, defined as the right-hand side of Eq. (10),

$$P = (1 + m_{12}\cos 2\gamma + m_{13}\sin 2\gamma), \quad (11)$$

is shown in Fig. 5 as solid curves. Using the trigonometric relation

$$\cos(x - y) = \cos(x)\cos(y) + \sin(x)\sin(y), \quad (12)$$

one can see that Eq. (10) is related to Eq. (1) with

$$p_a = \sqrt{{m_{12}}^2 + {m_{13}}^2},$$

$$m_{12} = -p_a \cos(2\delta),$$

$$m_{13} = p_a \sin(2\delta). \quad (13)$$

Table 2 lists polarization amplitudes p_a for the MODIS Aqua ocean color bands, averaged over all viewing angles, and the maximum values, which typically occur at the largest viewing angles where measurements were taken (45°), corresponding to a large AOI on the scan mirror. The values of bands 8 and 9 have been increased by 10% relative to the fitted values [e.g., mean(p_a) of band 8 was increased from 4.5% to 5.0%] to adjust for an expected decrease in the degree of polarization of the PSA for shorter wavelengths. The table also contains average polarization phase angle δ, which corresponds to the polarizer rotation angle β with the highest measured radiances I_m^N; see Eq. (1). The polarization phase angle of band 12 is substantially different from the phase angles of bands 8–11. We plan to investigate whether this difference is supported by MODIS on-orbit data.

Polarization coefficients m_{12} and m_{13} are applied to correct the measured TOA radiances I_m by use of Eq. (5). Figure 9 provides information on the polarization correction of the MODIS Aqua 412 nm band for a swath over the Pacific Ocean at an approximate longitude of 160° W for 14 August 2002. The equator is indicated by the horizontal white line. The measured TOA radiances I_m are shown in Fig. 9(a). The modeled Stokes polarization components (Rayleigh and glint) of the TOA radiance are shown in Figs. 9(b) (Q_t) and 9(c) (U_t). Figure 9(d) shows the degree of polarization d_p, defined as[21]

$$d_p = \sqrt{{Q_t}^2 + {U_t}^2}/I_t, \quad (14)$$

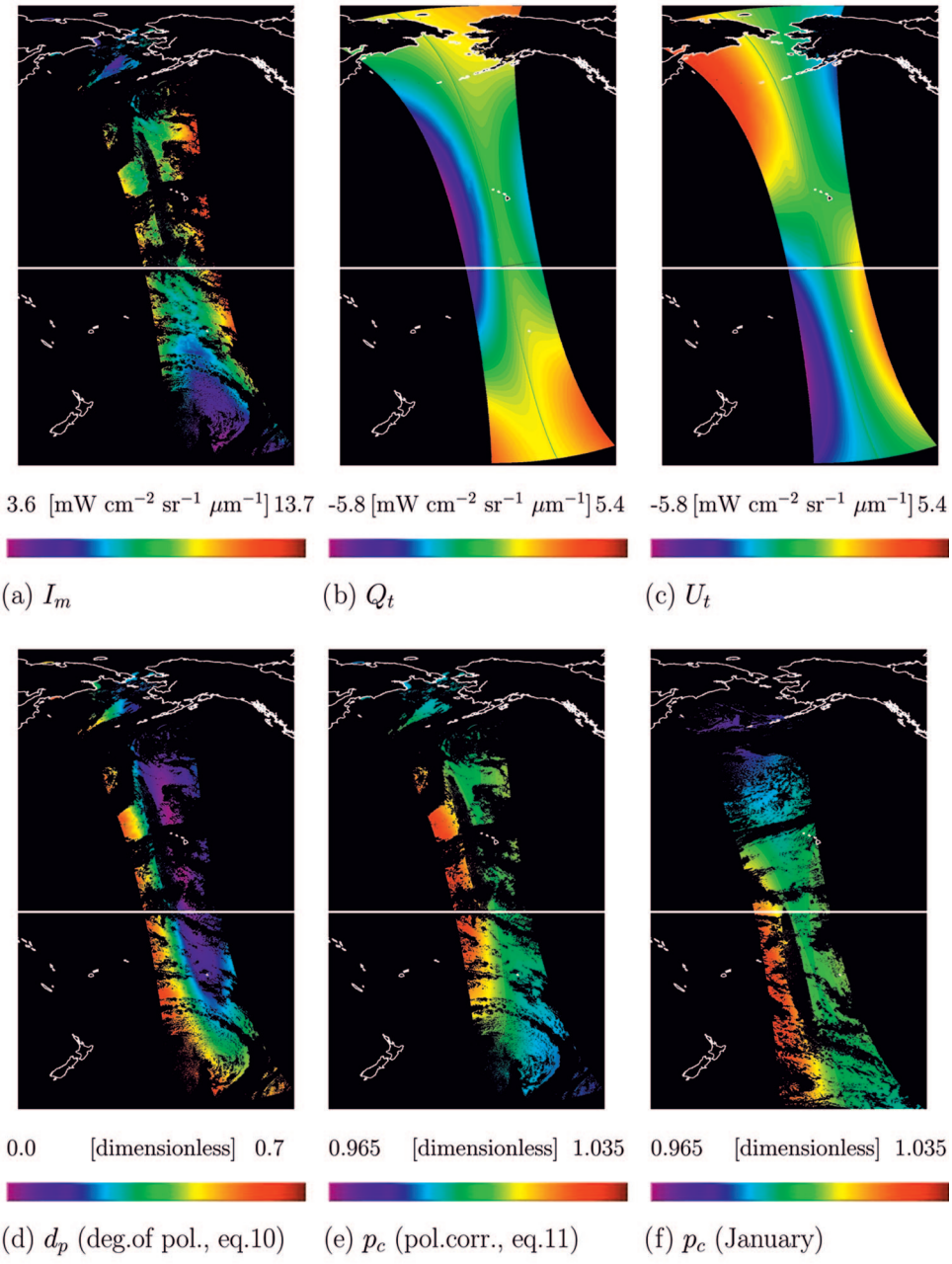

Fig. 9. Polarization correction for MODIS Aqua band 8 (412 nm) for (a)–(e) a swath over the Pacific Ocean on 14 August 2002; (f) is for 18 January 2003.

where I_t is the corrected TOA radiance. The degree of polarization varies from 0 to ~70% and describes the modeled polarization of the TOA radiance. This quantity does not directly determine the polarization correction, as can be seen from Eq. (6); it is shown here for illustrative purposes only. The MODIS polarization correction coefficients m_{13} are usually much smaller than the coefficients m_{12}; thus the Q_t component influences the polarization correction much more than the U_t component. The polarization correction p_c is defined here as

$$p_c = I_m/I_t. \tag{15}$$

Equation (6) implies that p_c for $\alpha = 0°$ can be calculated from

$$p_c = 1 + m_{12}Q_t/I_t + m_{13}U_t/I_t. \tag{16}$$

However, only I_m is known initially for a MODIS on-orbit measurement, whereas I_t is the quantity that we want to derive by using p_c. It is easy to show that, for $\alpha = 0°$, p_c can also be calculated from

$$p_c = \frac{1}{1 - m_{12}Q_t/I_m - m_{13}U_t/I_m}. \tag{17}$$

For $\alpha \neq 0°$, Eq. (17) becomes

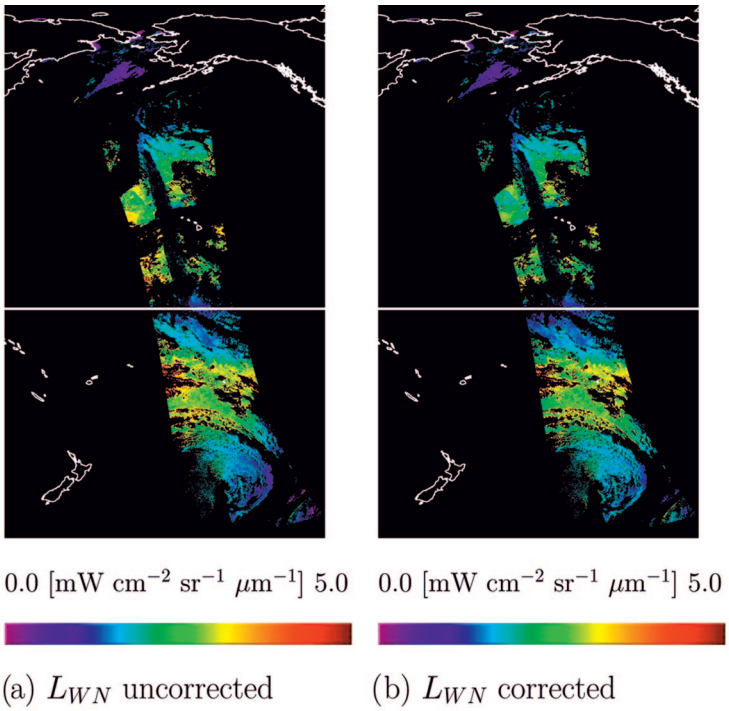

Fig. 10. MODIS Aqua band 8 L_{WN} (412 nm) for a swath over the Pacific Ocean on 14 August 2002.

$$p_c = \frac{1}{1 - m_{12}[\cos(2\alpha)Q_t + \sin(2\alpha)U_t]/I_m - m_{13}[-\sin(2\alpha)Q_t + \cos(2\alpha)U_t]/I_m}. \quad (18)$$

Equation (18) is the current implementation for the calculation of p_c. In the original implementation of the polarization correction, I_t in Eq. (16) was replaced by I_m. The difference between the two algorithms is small, with a mean absolute difference of less than 0.2% on a global data set.

Polarization correction p_c is shown in Fig. 9(e). Polarization amplitude p_a of band 8 (see Fig. 7) increases toward the end of the scan (toward the left in Fig. 9); thus Fig. 9(e) looks similar to Fig. 9(b) but with a stronger gradient and inverted, because m_{12} is negative. p_c ranges from 0.982 to 1.034 for this scene.

The effect on the most sensitive water-leaving radiance, L_{WN} (412 nm) for this scene, can be seen by comparison of the uncorrected L_{WN} in Fig. 10(a) (derived from I_m) to the corrected L_{WN} in Fig. 10(b) (derived from I_t). In general, differences between the west side of the scan and the east side of the scan have been reduced by the polarization correction. Note that around the equator the L_{WN} are more homogeneous across the swath in the corrected image (similar amounts of blue pixels in east and west), whereas in the uncorrected image the L_{WN} values are higher on the west side of the scan. Note also that the

Table 3. Global TOA Polarization Correction p_c [Eq. (15)] and Estimated Standard Uncertainties (k = 1) for the Mean Polarization Correction σ[mean(p_c)] and the Strongest Polarization Correction σ[max($\|p_c - 1\|$)][a]

Band	Mean($\|p_c - 1\|$)	σ[mean($\|p_c - 1\|$)]	Max($p_c - 1$)	Min($p_c - 1$)	σ[max($\|p_c - 1\|$)]
8	0.006	<0.001	0.032	−0.022	0.001
9	0.004	0.001	0.020	−0.010	0.003
10	0.002	0.001	0.007	−0.006	0.006
11	0.002	0.001	0.009	−0.004	0.006
12	0.002	0.001	0.011	−0.006	0.003
13L	0.001	0.002	0.005	−0.002	0.006
15	0.001	0.001	0.004	−0.003	0.005
16	0.002	<0.001	0.008	−0.016	0.003

[a]The statistics for p_c were calculated from a representative global subset for 14 August 2002. The processing for band 14 had not been implemented as of the writing of this paper.

very low L_{WN} region in the southeast of the uncorrected image (purple color) is much smaller in the corrected image. The correction increased the L_{WN} in the southeast of the image by ~ 0.3 mW cm^{-2} sr^{-1} μm^{-1} and decreased the L_{WN} on the west side of the scan by ~ 0.3 mW cm^{-2} sr^{-1} μm^{-1}. Over the whole image, the correction varies between a decrease of 1.1 mW cm^{-2} sr^{-1} μm^{-1} to an increase of 1.3 mW cm^{-2} sr^{-1} μm^{-1}.

A common problem of atmospheric correction for ocean color is that, for some pixels, the calculated L_{WN} (412 nm) is negative. For the uncorrected data shown in Fig. 10(a), the percentage of negative L_{WN} is 0.4%; for the corrected data in Fig. 10(b) it is 0.2%. This is an indication that the polarization correction improves the data quality.

The mean degree of polarization d_p of the data shown in Fig. 9(d) is 0.25, but the mean d_p of the negative L_{WN} (after polarization correction) is 0.44. Thus it is likely that residual problems in the polarization correction contribute to the occurrence of negative L_{WN}.

Global statistics for polarization correction p_c for all ocean color bands are given in Table 3. Band 8 TOA radiances are affected the most, with a mean correction of 0.6% and a range of corrections of 5.4% (from $p_c = 1.032$ to $p_c = 0.978$). Note that mean correction is defined here as mean($\|p_c - 1\|$) to prevent the cancellation of values of $p_c > 1$ and $p_c < 1$ in the average. Bands 13 and 15 have the lowest range of corrections of 0.7%. The range of the band 16 polarization corrections is 2.4%. The atmospheric correction typically accounts for 90% of the signal and therefore has a large effect on the retrieved L_{WN}. Furthermore, as Fig. 5 shows, the MODIS polarization sensitivity of band 8 (and most other ocean color bands) is opposite in phase to that of band 16, which leads to an increase in the polarization sensitivity of the MODIS L_{WN}. The error in the ocean color products when the MODIS polarization sensitivity has not been corrected for is described in Section 4 in more detail.

We also estimated the uncertainties for the TOA radiances that are due to uncertainties in correction coefficients m_{12} and m_{13} derived with Eq. (10). In a first step, we estimated the uncertainty of modeled polarization sensitivity σ_P [see Eq. (11)] for each band. These uncertainties are given in Table 2. These estimates are based only on the reliability of the fit of the modeled polarization sensitivity to the measured radiances (see, e.g., Fig. 5) and do not include systematic biases in our algorithm, e.g., the assumption that all detectors of one band have the same polarization sensitivity or our assumption regarding the degree of polarization of the light produced by the PSA. Therefore these estimated uncertainties are probably lower than the true uncertainties. We then estimated how σ_P affects the uncertainty of the mean polarization correction σ[mean($\|p_c - 1\|$)] and the uncertainty of the strongest polarization correction σ[max($\|p_c - 1\|$)]. Future research may lead to an improved understanding of the prelaunch measurements and possibly to a downward revision of the uncertainty estimates.

Polarization correction uncertainties are given in Table 3. A typical value for the mean uncertainty of a TOA radiance owing to uncertainty in the polarization correction coefficients is 0.1%. Table 3 also shows that the accuracy goal for TOA radiances of 0.5% is unattainable for those pixels of bands 10, 11, 13, and 15 with the strongest polarization correction {with σ[max($\|p_c - 1\|$)] from 0.5% to 0.6%}, whereas the uncertainty of the mean polarization correction does not by itself breach that goal for any band {σ[mean($\|p_c - 1\|$)] $\leq$ 0.2%}.

For some bands, the mean polarization correction is similar in magnitude to the polarization uncertainty. This does not mean that it is superfluous to apply this correction, because the true polarization correction of those bands is as likely to be either negligible or twice the currently applied magnitude. In other words, the currently applied correction is that which is most likely to be the correct one, according to our current state of knowledge. It is worth noting that the signal-to-noise ratio of the MODIS ocean color bands[3] has a magnitude similar to that of the uncertainty for the mean polarization correction. But, unlike uncertainty from noise, the polarization correction uncertainty can potentially lead to systematic biases.

The uncertainty estimate presented in Table 3 does not include uncertainties of the atmospheric correction algorithm. According to Gordon *et al.*,[10] the atmospheric correction at 443 nm does not perform well if the polarization sensitivity in this band is opposite in phase to the atmospheric correction bands and the polarization amplitude is 0.02 or larger. MODIS bands 8, 9, and 16 have polarization amplitudes of $\sim$0.02 or larger (see Table 2), and the phase of the polarization sensitivity of band 16 is opposite that of bands 8 and 9, as can be seen from Fig. 5: For angles β for which the measured radiances of band 8 are high, the radiances of band 16 are low, and vice versa. Band 9 is similar in phase to band 8; cf. δ in Table 2. Thus, although the estimated uncertainties σ[mean($\|p_c - 1\|$)] in Table 3 are lower in bands 8 and 9 than in bands 10–12, this does not imply that the polarization correction performance is better for the L_{WN} of bands 8 and 9 than for the L_{WN} of bands 10–12, whose polarization amplitude is only $\sim$0.01. The negative L_{WN} (412 nm) in the polarization corrected data discussed above are probably caused partly by problems for bands with a high polarization amplitude of the atmospheric correction algorithm.

4. Comparison of MODIS Aqua and SeaWiFS

In this section we show the importance of the MODIS polarization correction by comparing MODIS level 3 data and level 3 data from the SeaWiFS.[11] It is difficult to compare the TOA radiances from the MODIS directly with those of other satellites, because usually the viewing geometries are different and the overpasses are not simultaneous. A feasible method for

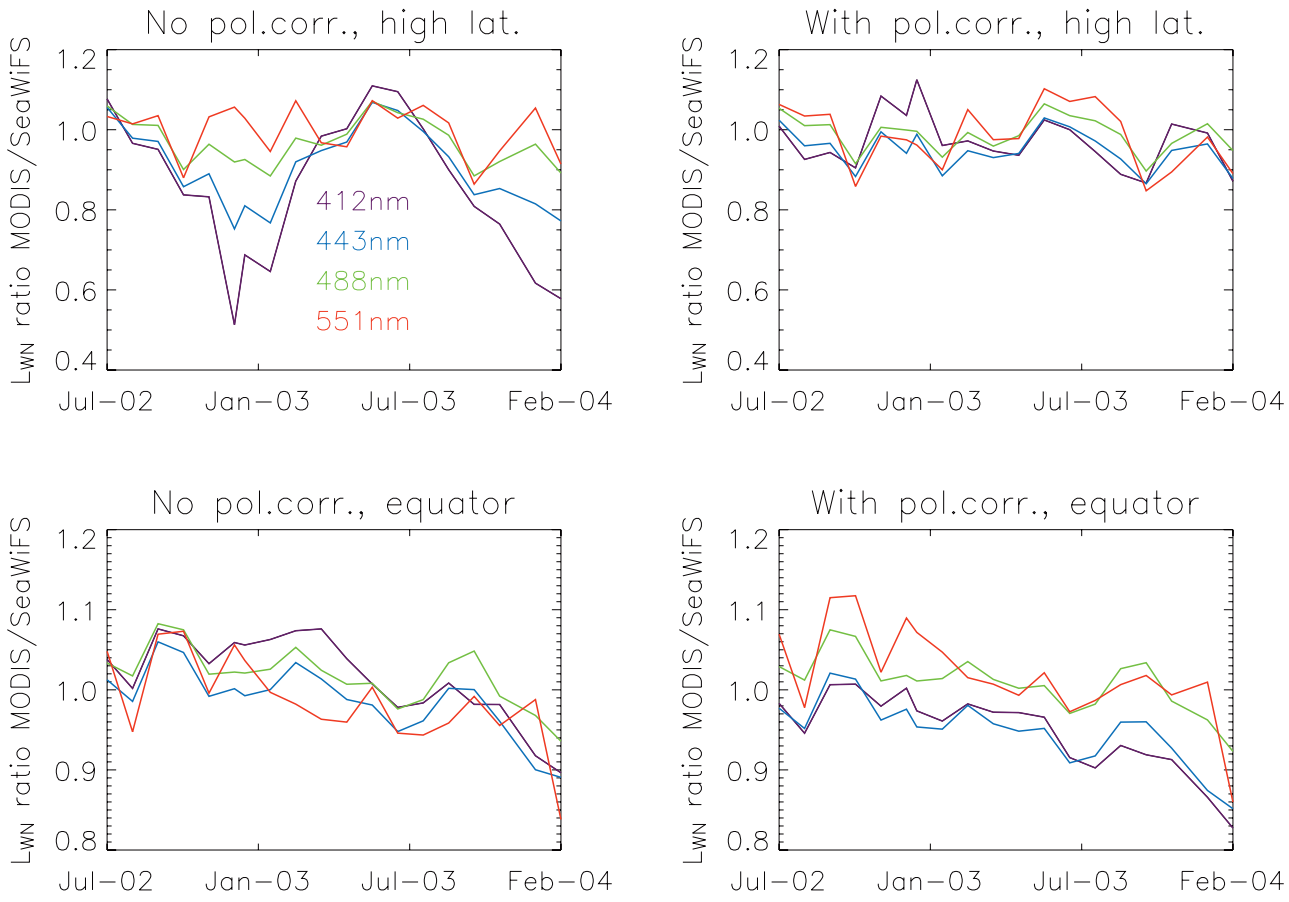

Fig. 11. Comparison of the L_{WN} ratio of MODIS Aqua and SeaWiFS for high latitudes and the equator, with and without polarization correction.

comparing data from different satellites is to use products derived from the TOA radiances that are independent of viewing geometry and do not change significantly between the overpasses, such as L_{WN}.

The MODIS Aqua and SeaWiFS ocean color products are produced with almost identical algorithms.[22–24] At present, it is unclear whether the remaining differences between the products from the two sensors are calibration artifacts or unaccounted-for geophysical effects, e.g., bidirectional ocean reflectance. The local overpass time for SeaWiFS (descending orbit) is close to noon, whereas for the MODIS Aqua (ascending orbit) it is ~1:30 PM. The resultant differences in viewing and illumination geometry are assumed to be removed from the basic ocean color product, the normalized water-leaving radiances L_{WN}.

In this section we compare the L_{WN} averaged over large ocean areas and 4 consecutive days for the two sensors, with and without applying the MODIS polarization correction. The L_{WN} were spatially averaged to approximately 9.3 km × 9.3 km equal-area bins,[25] and only bins with common coverage for both sensors were used for the calculation of the averages. For algorithm and calibration testing, the OBPG processes a temporal subset of the mission life-span consisting of 4 day global composites generated from the start of each consecutive 32 day period (i.e., 12.5% of the mission data set). The 4 day compositing period generally provides sufficient opportunity to observe most of the daylit side of the Earth, including coverage in orbit and glint gaps. The temporal subset can usually be processed within 1 day, so it allows for rapid analysis of processing changes on global spatial scales and life-of-mission time spans.

The SeaWiFS optics include a polarization scrambler; thus its polarization sensitivity is negligible compared with that of the MODIS.[26] This makes the SeaWiFS data set a good candidate for evaluating changes in the MODIS polarization correction.

A comparison of the spectral bandpasses of ocean color bands for the two sensors is given in Table 1. The 750/765 nm and 870 nm bands are used for the atmospheric correction of the other bands because their L_{WN} are very low and thus cannot be used for L_{WN} comparisons. There is no SeaWiFS band that has a wavelength similar to the MODIS band 11. The SeaWiFS 670 nm band has significantly more noise than the other SeaWiFS bands, and the signal at 670 nm is quite small in the open ocean; thus the L_{WN} comparisons in this section are limited to the 412, 443, 488, and 551 nm bands.

The left-hand side of Fig. 11 shows the L_{WN} ratios for the MODIS Aqua and the SeaWiFS without po-

larization correction from July 2002 to February 2004 for the four bands mentioned above. The L_{WN} have been averaged over 4 days for each month in this time period, for latitudes from 30° N to 50° N at high latitudes (top) and from 10° S to 10° N near the equator (bottom). The longitude range for both regions is 150° W to 170° W. The right-hand side of the figure shows the ratio of MODIS L_{WN} with polarization correction to the SeaWiFS L_{WN}.

The importance of the polarization correction is seen when one compares the ratios with and without the polarization correction for the northern high-latitude region: Using the polarization correction significantly improves the agreement of the L_{WN} from the MODIS and the SeaWiFS. For the 412 nm band, the 50% decrease of the ratio during the Northern Hemisphere winter has been removed. The ratios of all bands are more nearly correlated with one another when the polarization correction is used. The effect of the polarization correction on the stability of the time trends is relatively small at the equatorial region. The reason can be understood when one compares polarization corrections p_c in Figs. 9(e) and 9(f): The polarization correction is similar in August and January at the equatorial region but opposite at high latitudes; for latitudes from 30° N to 50° N (south of Alaska's Aleutian Islands), Fig. 9(e) varies from green to red (i.e., $p_c > 1$), whereas Fig. 9(f) is predominantly blue (i.e., $p_c < 1$).

There is a downward trend with time in most ratios shown in Fig. 11, especially in the 412 nm band ratio. This was probably a result of a time trend in the radiometric calibration of the MODIS and has been resolved with more-recent models of the radiometric degradation of the MODIS.

Note that the ratios of the 488 and 551 nm bands in the equatorial region are higher by ~5% than the ratios of the 412 and 443 nm bands when the polarization correction is used. This is an expected result from the wavelength differences between the MODIS and SeaWiFS bands; see Franz *et al.*[27] The expected difference decreases for higher chlorophyll concentrations. The difference does not appear in the ratios of the data without polarization correction. It is possible that the vicarious gains[9] of the data set without polarization correction (which presumably are inferior to the vicarious gains derived with polarization correction) prevent the appearance of the difference. The difference does not appear in the high-latitude area when the polarization correction is used, probably because chlorophyll concentrations for the high-latitude Pacific are generally higher than for the equatorial Pacific.

5. Conclusions and Outlook

The polarization characterization of a large aperture instrument such as the MODIS is a technological challenge. In this paper we have highlighted several problems of the prelaunch characterization measurements; see Figs. 4–6 (detector variations, lack of two-cycle pattern, four-cycle effect). However, there is now no clear evidence that the derived polarization correction yields significantly incorrect results for the MODIS Aqua ocean color products. These products are highly sensitive to polarization because ~90% of the signal in the ocean color bands is due to the atmosphere, which often includes a highly polarized contribution from Rayleigh scattering. In effect, the current polarization correction is essential for the good agreement between the MODIS Aqua and SeaWiFS time series, especially for the short wavelengths at high latitudes; see Fig. 11. The polarization correction significantly reduces the occurrence of negative L_{WN} at 412 nm.

For most ocean color bands, the typical mean TOA radiance polarization correction is ~0.2%, and the maximum polarization correction is ~1%; see Table 3. Bands 8 and 9 have significantly higher corrections. Globally, the range of variation of the polarization correction varies from 0.7% (bands 13 and 15) to 5.4% (band 8) for the MODIS Aqua ocean color bands. The strong spatial and temporal variations of the band 8 polarization correction are shown in Figs. 9(e) and 9(f).

The current implementation of the polarization correction is entirely based on the prelaunch polarization measurements. Future implementations may be based on an improved understanding of the MODIS polarization sensitivity derived from ray tracing models or from pixel-based comparisons to SeaWiFS, which may provide detector-specific polarization coefficients, a time-varying polarization sensitivity that reflects the on-orbit degradation[28] of the MODIS optics, or a different algorithm to process the prelaunch measurements.

The polarization characteristics of aerosols are ignored in the current processing. Howard Gordon (hgordon@miami.edu) of the University of Miami is working on aerosol scattering models to include these effects. The models will provide the Q_t and U_t polarization components produced by aerosol scattering for TOA radiances. These components will be added to the polarization components produced by Rayleigh scattering and glint. Other refinements in the processing, such as the improvement of ocean bidirectional reflectance distribution function BRDF corrections, are being assessed as well.

We thank Eugene Waluschka, Code 551, NASA, for his efforts in determining the setup of the MODIS prelaunch polarization characterization experiment and Howard Gordon of the University of Miami for his explanations of the polarization correction algorithm. We are also thankful to the MODIS characterization support team, to the remaining members of the OBPG at NASA's Goddard Space Flight Center, to the MODIS polarization ray trace group, and to SBRS staff members James Young, Milutin Pavlov, Roger Drake, and Edward Knight of Ball Aerospace for helpful comments. The comments of two anonymous reviewers significantly improved this paper. This research was funded by the NASA MODIS Science Team.

References

1. Y. J. Kaufman, D. D. Herring, K. J. Ranson, and G. J. Collatz, "Earth Observing System AM1 mission to Earth," IEEE Trans. Geosci. Remote Sens. **36,** 1045–1055 (1998).
2. C. L. Parkinson, "Aqua: an Earth-Observing Satellite mission to examine water and other climate variables," IEEE Trans. Geosci. Remote Sens. **41,** 173–183 (2003).
3. W. L. Barnes, T. S. Pagano, and V. V. Salomonson, "Prelaunch characteristics of the Moderate Resolution Imaging Spectroradiometer (MODIS) on EOS-AM1," IEEE Trans. Geosci. Remote Sens. **36,** 1088–1100 (1998).
4. G. C. Feldman, "Ocean color home page," http://oceancolor.gsfc.nasa.gov/.
5. E. J. Knight, C. Merrow, and C. Salo, "Interaction between polarization and response vs. scan angle in the calibration of imaging radiometers," in *Polarization: Measurement, Analysis, and Remote Sensing II*, D. H. Goldstein and D. B. Chenault, eds., Proc. SPIE **3754,** 308–319 (1999).
6. M. Wang, B. A. Franz, R. A. Barnes, and C. R. McClain, "Effects of spectral bandpass on SeaWiFS-retrieved near-surface optical properties of the ocean," Appl. Opt. **40,** 343–348 (2001).
7. H. R. Gordon and M. Wang, "Surface-roughness considerations for atmospheric correction of ocean color sensors. I. The Rayleigh-scattering component," Appl. Opt. **31,** 4247–4260 (1992).
8. M. Wang, "The Rayleigh lookup tables for the SeaWiFS data processing: accounting for the effects of ocean surface roughness," Int. J. Remote Sens. **23,** 2693–2702 (2002).
9. H. R. Gordon, T. Du, and T. Zhang, "Atmospheric correction of ocean color sensors: analysis of the effects of residual instrument polarization sensitivity," Appl. Opt. **36,** 6938–6948 (1997).
10. R. E. Eplee, Jr., W. D. Robinson, S. W. Bailey, D. K. Clark, P. J. Werdell, M. Wang, R. A. Barnes, and C. R. McClain, "Calibration of SeaWiFS. II. Vicarious techniques," Appl. Opt. **40,** 6701–6718 (2001).
11. C. R. McClain, G. C. Feldman, and S. B. Hooker, "An overview of the SeaWiFS project and strategies for producing a climate research quality global ocean biooptical time series," Deep-Sea Res. II **51,** 5–42 (2004).
12. B. Guenther, W. Barnes, E. Knight, J. Barker, J. Harnden, R. Weber, M. Roberto, G. Godden, H. Montgomery, and P. Abel, "MODIS calibration: a brief review of the strategy for the at-launch calibration approach," J. Atmos. Ocean. Technol. **13,** 274–285 (1996).
13. B. Guenther, G. D. Godden, X. Xiong, E. J. Knight, S. Qiu, H. Montgomery, M. M. Hopkins, M. G. Khayat, and Z. Hao, "Prelaunch algorithm and data format for the Level 1 calibration products for the EOS-AM1 Moderate Resolution Imaging Spectroradiometer (MODIS)," IEEE Trans. Geosci. Remote Sens. **36,** 1142–1150 (1998).
14. E. Waluschka, "MODIS polarization measurements and simulation and the 4θ effect," in *Polarization: Measurement, Analysis, and Remote Sensing*, D. H. Goldstein and R. A. Chipman, eds., Proc. SPIE **3121,** 278–287 (1997).
15. J. P. Bauer, "FM1 Polarization Insensitivity Summary (PC-08)," Raytheon Interdepartmental Correspondence, Raytheon Company, Ref. PL3095-N08165 (1 February 2000).
16. G. Meister, "Derivation of Aqua MODIS polarization correction," http://oceancolor.gsfc.nasa.gov/ocvalidation.html (June 2004).
17. N. Souaidia, D. Moyer, E. Waluschka, and K. Voss, "MODIS polarization ray tracing analysis," presented at the SPIE Symposium on Optics and Photonics, San Diego, Calif., 31 July–4 August 2005.
18. J. Young, E. Knight, and C. Merrow, "MODIS polarization performance and anomalous four-cycle polarization phenomenon," in *Earth Observing Systems III*, W. L. Barnes, ed., Proc. SPIE **3439,** 247–256 (July 1998).
19. S. Chandrasekhar, *Radiative Transfer* (Dover, 1960).
20. S. J. Kempler, "GES DISC DAAC," http://daac.gsfc.nasa.gov/.
21. E. Collett, *Polarized Light* (Marcel Dekker, 1992).
22. B. A. Franz, "Overview of MODIS processing within the ocean color discipline processing system (OCDPS)," http://oceancolor.gsfc.nasa.gov/DOCS/modis_processing_overview.pdf (accessed July 2004).
23. M. Wang, "A sensitivity study of the SeaWiFS atmospheric correction algorithm: effects of spectral band variations," Remote Sens. Environ. **67,** 348–359 (1999).
24. H. R. Gordon and M. Wang, "Retrieval of water-leaving radiance and aerosol optical thickness over the oceans with SeaWiFS: a preliminary algorithm," Appl. Opt. **33,** 443–452 (1994).
25. J. W. Campbell, J. M. Blaisdell, and M. Darzi, "Level-3 SeaWiFS data products: spatial and temporal binning algorithms," S. B. Hooker, E. R. Firestone, and J. G. Acker, eds., NASA Tech. Memo. 104566 (1995), Vol. 32.
26. R. A. Barnes, W. L. Barnes, W. E. Esaias, and C. R. McClain, "Prelaunch acceptance report for the SeaWiFS radiometer," Vol. 22, S. B. Hooker, E. R. Firestone, and J. G. Acker, eds., NASA Tech. Memo. 104566 (1994), Vol. 22.
27. B. A. Franz, S. W. Bailey, R. E. Eplee, Jr., G. C. Feldman, E. Kwiatkowska, C. McClain, G. Meister, F. S. Patt, D. Thomas, and P. J. Werdell, "The continuity of ocean color measurements from SeaWiFS to MODIS," presented at the SPIE Symposium on Optics and Photonics, San Diego, Calif., 31 July–4 August 2005.
28. X. Xiong, A. Wu, J. A. Esposito, J. Sun, N. Che, B. Guenther, and W. Barnes, "Trending results of MODIS optics on-orbit degradation," in *Earth Observing Systems VII*, W. L. Barnes, ed., Proc. SPIE **4814,** 337–346 (2002).